

Indirect probing of light-induced nonadiabatic dynamics in lossy nanocavities

Krisztián Szabó,[†] Csaba Fábri,[†] Gábor J. Halász,[‡] and Ágnes Vibók^{*,†,¶}

[†]*Department of Theoretical Physics, University of Debrecen, P.O. Box 400, H-4002 Debrecen, Hungary*

[‡]*Department of Information Technology, University of Debrecen, P.O. Box 400, H-4002 Debrecen, Hungary*

[¶]*ELI-ALPS, ELI-HU Non-Profit Ltd, H-6720 Szeged, Dugonics tér 13, Hungary*

E-mail: vibok@phys.unideb.hu

Abstract

Light-induced nonadiabatic effects can arise from the interaction of a molecule with the quantized electromagnetic field of a Fabry–Pérot or plasmonic nanocavity. In this context, the quantized radiation field mixes the vibrational, rotational, and electronic degrees of freedom. In this work, we investigate the photodissociation dynamics of a rotating hydrogen molecule within a lossy plasmonic nanocavity. We highlight that, due to significant cavity loss, the dynamics are governed by an infinite number of light-induced conical intersections. We also examine the dissociation dynamics of fixed-in-space molecules by neglecting rotation, employing both the Lindblad master and non-Hermitian lossy Schrödinger equations. Additionally, we incorporate the effects of rotation within the parameter range of perfect agreement using the non-Hermitian lossy Schrödinger method. Furthermore, we show that in the absence of photon losses, there is a close correspondence between the classical Floquet description and the radiation field model.

Introduction

When molecules are placed into optical or plasmonic nanocavities, hybrid light-matter states, known as polaritons, are formed, exhibiting both excitonic and photonic characteristics. The electric dipole moment of the molecular system and the quantized radiation mode of the cavity can resonantly couple, which enables the manipulation and control of various physical and chemical properties of molecules. Numerous experimental studies^{1–13} and theoretical investigations^{14–40} have focused on molecular polaritons since the first pioneering experimental work reported by Ebbesen and coworkers.^{1,6} Among the key findings, the quantized radiation field has been shown to amplify⁴¹ or suppress¹⁵ well-known physical mechanisms and even induce novel effects. It can significantly alter the rate of spontaneous emission,⁴² energy transfer,^{43,44} and charge transfer processes.^{45–47} Moreover, strong light-matter coupling has the potential to modify chemical landscapes and reactions,^{16,48–51} influencing pro-

cesses such as photochemical reactivity,^{52,53} photoisomerization,^{54,55} photodissociation,^{56,57} photoionization,⁵⁸ and photoassociation.⁵⁹ Additionally, cavity-molecule coupling can induce nonadiabatic effects in molecules that are absent under field-free conditions.^{22,60–74} In these cases, the quantized radiation field can resonantly couple molecular electronic, vibrational, and rotational degrees of freedom (DOFs), leading to the formation of light-induced avoided crossings (LIACs) or light-induced conical intersections (LICIs)^{75–78}. In polyatomic molecules, a sufficient number of vibrational DOFs are always present to establish a two-dimensional branching space (BS) which is indispensable to form LICIs. In case of diatomic molecules, the rotational angle between the molecular axis and the polarization direction of the cavity field can serve as a dynamical variable to span the BS. A vast number of experimental and theoretical works have demonstrated that the LICIs has a remarkable impact on absorption spectra (e.g., intensity borrowing),^{22,58,79,80} topological properties (e.g., Berry phase),^{65,67} and quantum dynamics of molecules.^{61,68,70} However, light-induced nonadiabatic dissociative dynamics in a lossy plasmonic nanocavity has not been investigated yet. This paper aims to fill this gap.

To effectively manipulate and control molecular properties, it is essential to reach the strong coupling regime where the rate of energy exchange between the cavity photons and the molecule exceeds both the photon leakage rate and system dephasing. Strong coupling can be achieved either by allowing a large number of molecules to interact with the electromagnetic mode,^{19,81} or, in case of a single molecule, by using a subwavelength plasmonic nanocavity.² However, the latter often exhibits significant losses, which must be properly accounted for in the numerical treatment.^{52,57,81}

Typically, photon losses are modeled by coupling the cavity-molecule system to a dissipative Markovian environment, leading to the Lindblad master equation approach.^{56,57,70,82,83} In this framework, the time evolution of the system is described by propagating the density matrix according to the appropriate Lindblad master equation. Another common method is based on the non-Hermitian time-dependent Schrödinger equation (TDSE), although this

approach is not universally applicable. The two methods are rigorously equivalent only when the incoherent decay terms are absent from the dynamics. In such cases, the quantum system is confined to a specific excitation manifold (e.g., the singly-excited subspace, consisting of a ground-state molecule with one photon and an excited-state molecule with zero photons). Here, the dissipative effects are incorporated into the non-Hermitian Hamiltonian, which results in the loss of norm in the nuclear wave packet during TDSE time propagation. In a previous study,⁸⁴ we demonstrated the additional conditions required for the Lindblad and non-Hermitian TDSE approaches to yield comparable results.

In this study, we investigate the cavity-induced nonadiabatic photodissociation dynamics of the hydrogen (H_2) molecule. We perform both fixed-in-space and two-dimensional (2D) calculations where the molecular rotation is treated either as a fixed parameter ($\theta = 0$, with θ being the angle between the polarization direction of the cavity electric field and the molecular axis) or as a dynamical variable in the 2D case. Our primary focus is short-time dynamics, as conical intersections play a significant role on this timescale. It is worth noting that while the photodissociation process of H_2 has been explored within the molecular plasmonic framework,⁵⁷ previous studies have typically neglected the effect of rotational DOFs on nonadiabatic dynamics.

The objectives of this paper are twofold. First, we aim to study the cavity-induced nonadiabatic dynamics in a lossy plasmonic nanocavity. Such a study must be performed in 2D where LICIs appear. This will allow us to reveal the difference between the impact of the cavity-induced avoided crossings (LIACs) and of light-induced conical intersections (LICIs). Second, we also explore the dynamics in the absence of photon losses, which allows us to demonstrate the close similarity between the classical Floquet description and the radiation field model.⁷³

Theory and Computational Protocol

A molecule coupled to a single cavity mode can be described by the Hamiltonian

$$\hat{H} = \hat{T}_M + V_M + \hbar\omega_c \hat{a}^\dagger \hat{a} - \vec{E} \vec{\mu} (\hat{a}^\dagger + \hat{a}), \quad (1)$$

where \hat{T}_M denotes the kinetic energy operator of the molecule (including vibration and rotation as well), V_M is the potential energy surface (PES), ω_c is the cavity angular frequency, while \hat{a}^\dagger and \hat{a} are the creation and annihilation operators of the cavity mode, respectively. The electric field strength is denoted by \vec{E} and $\vec{\mu}$ stands for the transition dipole moment (TDM) of the molecule. We consider two electronic states of the hydrogen molecule, the ground electronic state $|X\rangle$ ($X^1\Sigma_g^+$) and the excited electronic state $|B\rangle$ ($B^1\Sigma_u^+$), both of which are singlet states. The PESs and TDM have been taken from Refs. 85, 86 and 87. We treat the light-matter interaction within the electric dipole approximation.

The polaritonic or dressed states can be calculated by diagonalizing the Hamiltonian of Eq. 1 without the kinetic energy term in the so-called singly-excited subspace which is spanned by the set $\{|X, 1\rangle, |B, 0\rangle\}$. We use the notation $|i, n\rangle = |i\rangle \otimes |n\rangle$ with $i = X, B$ and $n = 0, 1, \dots$ for the combined states of the molecule and cavity, where $|n\rangle$ denotes the Fock state of the cavity mode. In this case, the potential energy matrix has two eigenvalues for each nuclear configuration (R, θ) , which span two surfaces over the branching space: lower (LP) and upper polaritonic (UP) surfaces, shown in Fig. 1 (panel B).

The strong coupling regime (for a single molecule) can be reached using a plasmonic nanocavity which typically has a much shorter lifetime than the timescale of the molecular dynamics. Therefore, the dissipative nature of the cavity has to be taken into account. Under these conditions, the time evolution of the system is governed by the Lindblad master

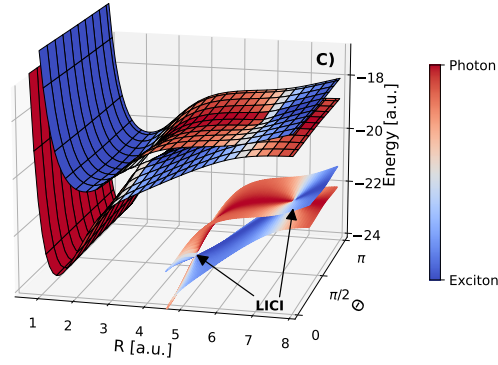
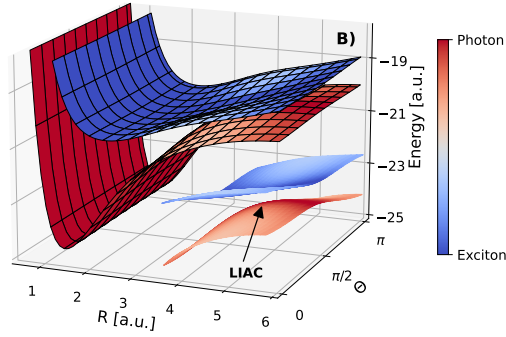
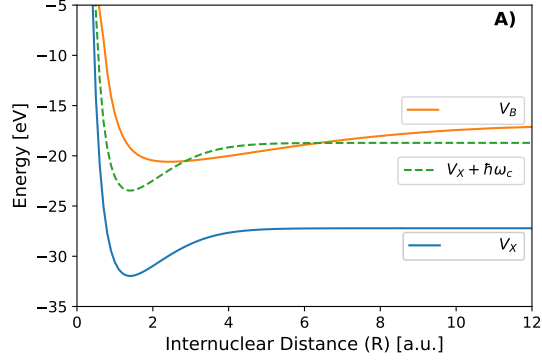


Figure 1: Potential energies of the H_2 molecule in a cavity. Panel A: Ground electronic state (denoted by V_X), first singlet excited electronic state (denoted by V_B) and potential energy curve corresponding to the molecule in ground electronic state and one photon in the cavity. The cavity central photon energy is $\hbar\omega_c = 7.4\text{ eV}$. Panel B: Two-dimensional polaritonic potential energy surfaces (PESs) along the vibrational and rotational coordinates of the H_2 molecule. The light-induced avoided crossing (LIAC) is highlighted in the inset on the right. The character of the polaritonic potential energy surfaces is indicated by different colors (see the legend on the right). The cavity central photon energy and field strengths are $\hbar\omega_c = 7.4\text{ eV}$ and $E = 300\text{ mV}/a_0 \approx 1.1 \cdot 10^{-2}\text{ a.u.}$. Panel C: Similar to panel B, but with cavity central photon energy of $\hbar\omega_c = 8.5\text{ eV}$. The light-induced conical intersections (LICIs) are highlighted in the inset on the right.

equation^{56,57,82-84}

$$\frac{\partial \hat{\rho}}{\partial t} = -\frac{i}{\hbar} [\hat{H}, \hat{\rho}] + \frac{1}{2} \sum_i \left(2\hat{C}_i \hat{\rho} \hat{C}_i^\dagger - \hat{\rho} \hat{C}_i^\dagger \hat{C}_i - \hat{C}_i^\dagger \hat{C}_i \hat{\rho} \right) \quad (2)$$

where $\hat{\rho}$ is the density operator describing the system, \hat{H} is the Hamiltonian and \hat{C}_i denotes collapse operators. We assume that the molecular excitations have infinite lifetime, hence only the cavity is coupled to the environment with $\hat{C}_c = \sqrt{\kappa} \hat{a}$, describing photon leakage to the environment. Here, the cavity decay rate κ ranges from 0 to 0.476 eV (equivalent to a finite photon lifetime $\tau = \hbar/\kappa$, e.g. $\kappa = 0.476$ eV $\rightarrow \tau \approx 1.38$ fs) and \hat{a} is the usual annihilation operator of the cavity mode. The Lindblad equation was solved within the QuTip framework^{88,89} (fixed-in-space model), where we used the truncated Hilbert space of $\{|X, 0\rangle, |X, 1\rangle, |B, 0\rangle, |B, 1\rangle\}$. The vibrational DOF (internuclear distance, denoted by R) was represented using a sine DVR (discrete variable representation) basis,⁹⁰ from $R = 0.5$ a.u. to $R = 17.0$ a.u. with $N = 200$ grid points, while the cavity mode was handled in the Fock representation.

Our simple case of a two-state hydrogen molecule with one cavity mode is already considered a challenging system. In special cases, the dynamics can be properly approximated with the time-dependent Schrödinger equation (TDSE) by incorporating an imaginary term in the Hamiltonian of Eq. (1). In our case the TDSE takes the form^{52,81,84}

$$i\hbar \frac{\partial |\Psi\rangle}{\partial t} = \left(\hat{H} - i\frac{\kappa}{2} \hat{N} \right) |\Psi\rangle. \quad (3)$$

The loss term works similarly to a complex absorbing potential (CAP), the flux absorption is proportional to the physical loss rate κ and the number of photons present in the cavity (given by the number operator $\hat{N} = \hat{a}^\dagger \hat{a}$). Of course, this is an approximation of the true Markovian interaction. It is also shown in Ref. 91 that the Lindblad master equation without the term $\kappa \hat{a} \hat{\rho} \hat{a}^\dagger$ is equivalent to the TDSE of Eq. (3). The term $\kappa \hat{a} \hat{\rho} \hat{a}^\dagger$ induces incoherent transitions $|\alpha(n+1)\rangle \rightarrow |\alpha n\rangle$ (α labels molecular electronic states X and B). The TDSE (see Eq. (3))

was solved with the multiconfiguration time-dependent Hartree (MCTDH) method.^{92,93} As basis, we used sine DVR for the vibrational DOF from $R = 0.5$ a.u. to $R = 17.0$ a.u. with $N = 500$ grid points, Legendre DVR for the rotational DOF with $N_\theta = 100$ grid points and Hermite DVR to describe the cavity mode with $N_c = 10$ grid points.

The dissociation of the H_2 molecule can lead to the reflection of the wave function at the edge of the grid, therefore we employ complex absorbing potentials (CAP) for each electronic state. The usual form of a CAP is⁹³

$$-iW(R) = -i\eta|R - R_c|^b\theta(R - R_c) \quad (4)$$

where R is the coordinate of the dissociative DOF, $\theta(x)$ denotes the Heaviside step function, η is a scalar, referred to as the strength of the CAP and R_c is the grid point where the CAP is switched on. Our parameters are chosen as $\eta = 10^{-4}$, $R_c = 12$ a.u. and $b = 4$.

The Lindblad equation describes strictly trace-preserving dynamics, which means that the Hamiltonian used in Eq. (2) must be Hermitian. Therefore, one can not use a CAP (see Eq. (4)) in this case. We can overcome this issue with a series of collapse operators, each couples one grid point to a special basis function $|\mathcal{D}\rangle$, with coupling strength proportional to $W(R_i)$ of Eq. (4) with R_i being the coordinate of the given grid point. The absorbing potential used in the Lindblad method, equivalent to the CAP of Eq. (4), is given by the series of collapse operators⁸⁹

$$C_{\text{Abs}} := \{\sqrt{2W(R_i)}|\mathcal{D}\rangle\langle R_i|\} \quad \forall i, R_i > R_c \quad (5)$$

where $|R_i\rangle$ is the internuclear DVR basis function corresponding to the grid point R_i .

The main observables we are interested in are the populations ($P_{A,i}$) and integrated dissociation probabilities ($P_{D,i}$). The population of states in case of the TDSE can be calculated as a simple inner product of the wave function corresponding to the given electronic state

at every time step,⁹⁴

$$P_{A,i}(t) = \langle \Psi_i(t) | \Psi_i(t) \rangle \quad (6)$$

where $i = X, B$. The integrated dissociation probability can be calculated through the so-called flux analysis method, which gives⁹³

$$P_{D,i}(t) = \int_0^t 2 \langle \Psi_i(t') | W | \Psi_i(t') \rangle dt' \quad (7)$$

where $i = X, B$. The same quantities have a slightly different formula if the system is described by the density operator. To calculate the dissociation probability, we use the state $|\mathcal{D}\rangle$ introduced in Eq. (5),⁹⁴

$$P_{D,|i,n\rangle}(t) = (\langle \mathcal{D} | \otimes \langle i, n |) \rho(t) (|i, n\rangle \otimes |\mathcal{D}\rangle) \quad (8)$$

where $i = X, B$ and $n = 0, 1$. The active or bound population can be expressed as⁹⁴

$$P_{A,|i,n\rangle}(t) = \langle i, n | \text{Tr}_{\text{DVR}} [\rho(t)] | i, n \rangle - P_{D,|i,n\rangle}(t) \quad (9)$$

where $i = X, B$, $n = 0, 1$ and Tr_{DVR} stands for a trace over the DVR basis of the vibrational DOF. The last term above is a technical byproduct, required as a consequence of the introduction of the helper state $|\mathcal{D}\rangle$.

In case of the non-Hermitian TDSE we have no information about the state $|X, 0\rangle$ since its wave function was absorbed by the imaginary term. The population represented by these wave packets can be easily calculated as the missing total population of the other states: $P_{|X,0\rangle}(t) = 1 - \sum_{i=X,B} (P_{A,i}(t) + P_{D,i}(t))$. To approximate (without the actual wave function)

the bound and dissociation probabilities of $|X, 0\rangle$, we use the ratio

$$\xi = \frac{P_{D,|X,0\rangle}}{P_{A,|X,0\rangle} + P_{D,|X,0\rangle}}, \quad (10)$$

where the probabilities are obtained using the Lindblad method in which all (dynamically active) states are accessible. The ratio above depends heavily on the central photon energy $\hbar\omega_c$ and slightly on the electric field strength E . The ω_c dependence was mapped directly by performing full propagations with different photon energy values, however the slight field strength dependence taken into account approximately: we determine an effective field strength E_{eff} by the weighted average of $E \cos \theta$ with weights based on the angular distribution. Then, we use the ratio $\xi_{\omega_c, E_{\text{eff}}}$ (obtained from a fixed-in-space Lindblad calculation, with $\hbar\omega_c$ photon energy and $E = E_{\text{eff}}$ field strength) to approximate the population of $|X, 0\rangle$ as $P_{A,|X,0\rangle} \approx 1 - \xi \cdot P_{|X,0\rangle}$ and dissociation probability as $P_{D,|X,0\rangle} \approx \xi \cdot P_{|X,0\rangle}$.

Results and Discussion

We consider a H_2 molecule placed inside a cavity, focusing on its ground electronic state X ($X^1\Sigma_g^+$) and the excited electronic state B ($B^1\Sigma_u^+$), both of which are singlet states. The potential energy surfaces $V_X(R)$ and $V_B(R)$, are coupled by the cavity photon. As a result of cavity-molecule coupling, polaritonic states are formed. We use a cavity central photon energy of $\hbar\omega_c = 7.4 \text{ eV}$ because total dissociation occurs at maximum efficiency at this energy (as will be discussed later).

We explore the scenario described as follows. Initially, the molecule is prepared in the vibrational and rotational ground state of the electronic ground state. Then, to initiate the dynamics ultrafast vertical excitation of the wave packet is presumed from $V_X(R)$ to $V_B(R)$. Applying the Lindblad master equation, one can describe the temporal evolution of the nuclear wave packet dynamics for the fixed-in-space model. As the wave packet oscillates on the $|B, 0\rangle$ state, it reaches a region where the two diabatic states $|B, 0\rangle$ and $|X, 1\rangle$ are

closest (see Fig. 1, panel A). At this point, part of the population is transferred back to the $|X, 1\rangle$ photonic state. Due to the lossy nature of the cavity, the population then decays back from $|X, 1\rangle$ to the ground state $|X, 0\rangle$ where dissociation can take place.

Fig. 2 presents the population distributions and dissociation probabilities for the three diabatic states. Notably, no dissociation occurs from the $|B, 0\rangle$ state, and the population essentially vanishes from this state until approximately $t = 400$ fs. The population curve corresponding to the $|X, 1\rangle$ surface mirrors the shape of the population in the $|B, 0\rangle$ state but is roughly 20 times smaller in magnitude. However, from the intermediate $|X, 1\rangle$ state, the population rapidly decays to the ground state $|X, 0\rangle$, from which part of it dissociates and part of it remains bound. In the $|X, 0\rangle$ ground state, the population increases, reaching a maximum around $t = 70$ fs, and then decreases, stabilizing at a constant value by $t = 400$ fs. In contrast, the dissociation probability continues to rise slightly, reaching a maximum at around $t = 400$ fs, after which it becomes essentially saturated. The time evolution is displayed up to $t = 1000$ fs in Fig. 2.

For comparison, we repeated the simulation using the non-Hermitian TDSE approach, applying the same parameters as in the Lindblad scheme. The non-Hermitian TDSE allows for the inclusion of a greater number of nuclear DOFs (rotational and vibrational) in the quantum-dynamical description, owing to its lower computational cost compared to the Lindblad master equation. The results obtained from the non-Hermitian TDSE are in perfect agreement with those derived from the Lindblad equation (see Fig. 2). In this fixed-in-space non-Hermitian TDSE numerical description, the orientation of the molecular axis relative to the cavity mode polarization direction remains fixed ($\theta = 0$) throughout the simulation. However, to describe appropriately the light-induced nonadiabatic dynamics of the H_2 molecule and to form a two-dimensional branching space, it is necessary to extend the previous model by incorporating the rotational DOF.

Subsequently, using the same parameter set that yielded excellent agreement between the Lindblad and non-Hermitian TDSE schemes with fixed-in-space molecules, we performed

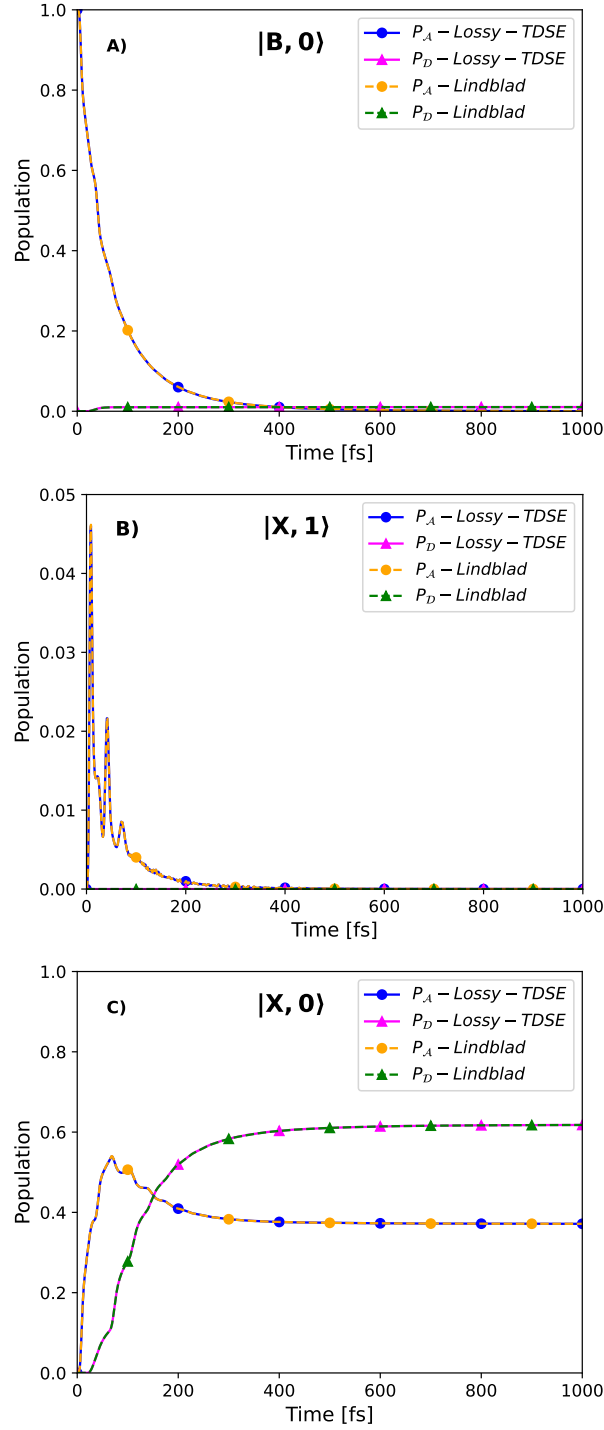


Figure 2: Populations (P_A) and dissociation probabilities (P_D) of the three different diabatic states (panel A: $|B, 0\rangle$ state, panel B: $|X, 1\rangle$ state and panel C: $|X, 0\rangle$ state) using the Lindblad and the non-Hermitian lossy Schrödinger schemes with fixed-in-space molecules. The parameters of the calculations are $\hbar\omega_c = 7.4$ eV (cavity central photon energy), $E = 70$ mV/a₀ $\approx 2.57 \cdot 10^{-3}$ a.u. (electric field strength) and $\kappa = 0.476$ eV ($\tau \approx 1.38$ fs).

two-dimensional (2D) simulations. In this case, the rotational DOF is treated as a dynamical variable during the numerical calculations. This extended model enables the inclusion of light-induced conical intersections (LICIs), thereby providing a more accurate treatment of nonadiabatic quantum dynamics. In the 2D model, LICIs are formed, as shown in panel C of Fig. 1. In the lossy cavity scenario, the photon energy undergoes broadening around the cavity central frequency, resulting in the appearance of an infinite number of photon energies at both lower and higher frequencies relative to the central frequency.^{57,95} At any given time, the nuclear dynamics are driven by this infinite set of light-induced conical intersections, formed by couplings at the corresponding photon energies. This situation is illustrated in Fig. 3 where the lower and upper polariton surfaces are shown for selected cavity frequencies in the range of $\hbar\omega_c = 6.8 \text{ eV} - 10 \text{ eV}$.

Let us now explore and discuss the fixed-in-space and 2D nuclear dynamics in the non-Hermitian lossy TDSE framework. It is well established that conical intersections primarily affect short-time dynamics, which is the reason why we restrict our analysis to the $t = 0 - 300 \text{ fs}$ time interval. The results are presented in Fig. 4. At first glance, it is striking that the $|X, 0\rangle$ state is populated significantly faster in the fixed-in-space model. Similarly, molecular dissociation begins more rapidly from the $|X, 0\rangle$ state in the fixed-in-space case. This is because the fixed-in-space scheme facilitates more efficient population transfer from the $|B, 0\rangle$ state to the $|X, 1\rangle$ state as the molecular axis remains parallel to the polarization direction of the cavity mode throughout the dynamics.

In contrast, the 2D model can be interpreted as capturing the combined effects of molecular rotation, light-induced conical intersections (LICIs) and the varying magnitudes and directions of the respective molecular transition dipole moments. As the nuclear wave packet oscillates on the $|B, 0\rangle$ state, the molecule rotates. When the wave packet reaches the coupling region, part of the population is transferred to the $|X, 1\rangle$ state. However, due to the rotation, the angle θ between the molecular transition dipole moment and the photon polarization axis changes continuously, causing the coupling strength to vary as well. As a result,

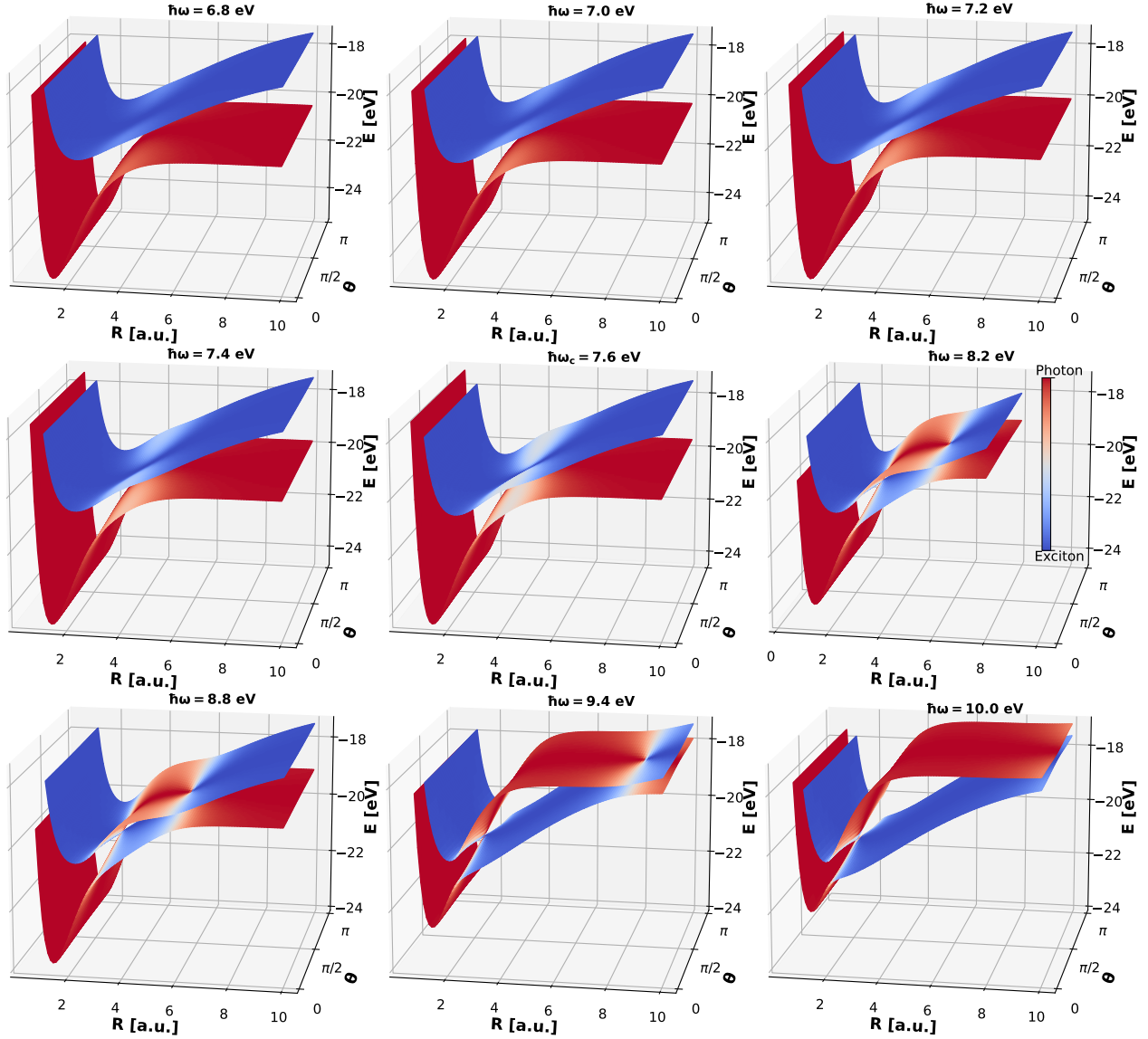


Figure 3: Two-dimensional polaritonic potential energy surfaces along the vibrational and rotational coordinates of the H_2 molecule. Figures are shown for $\hbar\omega_c = 7.6$ eV (cavity central photon energy) as well as for eight other energy values among the infinitely many that arise within the range of energy broadening. The $\hbar\omega_c = 7.6$ eV value is the resonance energy as well, because the two potential energy curves are the closest to each other here.

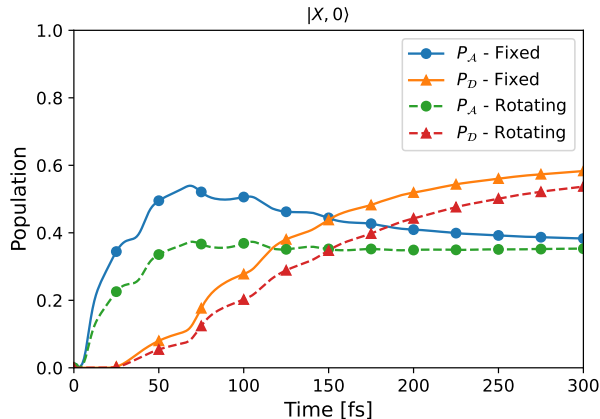


Figure 4: The active (P_A) and dissociated (P_D) populations of the $|X, 0\rangle$ state as a function of time obtained for the case of fixed-in-space and rotating H_2 molecules by using the non-Hermitian lossy TDSE. The parameters are the same as in Fig. 2.

less population is transferred to the $|X, 1\rangle$ state compared to the fixed-in-space case where the photon polarization and the molecular axis remain aligned.

Moreover, when the wave packet reaches the positions of the LICIs, nonadiabatic population transfer can take place between the upper and lower polaritonic states, allowing part of the population to transfer back from the $|X, 1\rangle$ state to the $|B, 0\rangle$ state. However, this effect is minor, as the population remains in the $|X, 1\rangle$ state only for a very brief period. The combined effect of these processes produces the 2D dynamical picture. Additionally, due to the lossy nature of the cavity, photon energy broadening results in the coupling of the $|X, 1\rangle$ and $|B, 0\rangle$ surfaces at a range of frequencies, not just the central frequency, further perturbing the dynamics. As is well known, the higher the quality of the cavity, the more the photon loss is concentrated around the cavity central frequency.⁹⁵

To proceed, we set several values for the central photon energy ranging from $\hbar\omega_c = 5$ eV to $\hbar\omega_c = 10$ eV and calculate the dissociation probabilities. As shown in Fig. 5, the results from the Lindblad and the non-Hermitian lossy Schrödinger equations with fixed-in-space molecules are nearly identical across all frequencies considered. This perfect agreement allows us to conclude that, for a given range of frequencies and parameters, the non-Hermitian Schrödinger equation provides an accurate description of the nonadiabatic dissociation dy-

namics. Using the non-Hermitian Schrödinger equation, we then compared the dissociation probabilities obtained from the fixed-in-space and 2D models. The results are shown in Fig. 6.

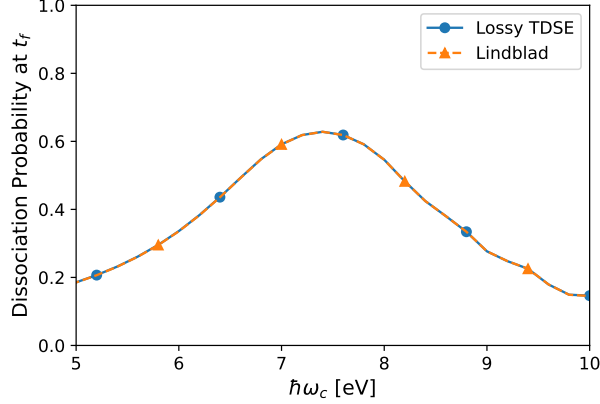


Figure 5: Dissociation probabilities (P_D) as a function of cavity central photon energy at $t_f = 1000$ fs obtained by the Lindblad and the non-Hermitian lossy Schrödinger schemes with fixed-in-space molecules. The central photon energy ranges from $\hbar\omega_c = 5$ eV to $\hbar\omega_c = 10$ eV with steps of $\Delta\hbar\omega_c = 0.2$ eV. The electric field strength and loss rate were kept at $E = 70$ mV/a₀ $\approx 2.57 \cdot 10^{-3}$ a.u. and $\kappa = 0.476$ eV ($\tau \approx 1.38$ fs), respectively.

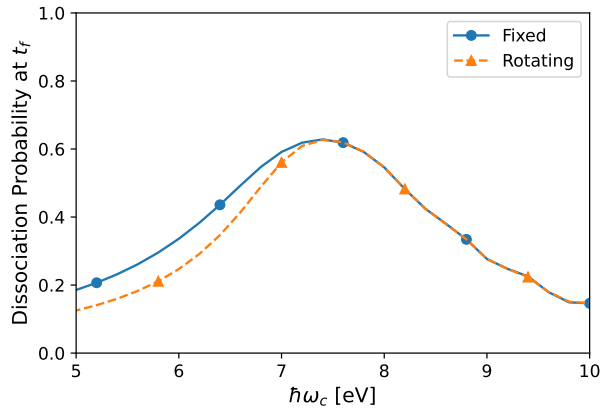


Figure 6: Dissociation probabilities (P_D) as a function of cavity central photon energy at $t_f = 1000$ fs obtained by the non-Hermitian lossy Schrödinger equation for the case of fixed-in-space and rotating molecules. Parameters are the same as in Fig. 5.

It is evident that both the fixed-in-space and 2D models predict the highest dissociation probability at central photon energy $\hbar\omega_c = 7.4$ eV. Interestingly, the two descriptions yield different results for energies below $\hbar\omega_c = 7.4$ eV, but they are quite similar for frequencies

above. This disparity arises because, for central energies lower than $\hbar\omega_c = 7.4$ eV, the photon energy broadening results in fewer coupling frequencies, which cannot fully compensate for the combined effects of molecular rotation and light-induced conical intersections (LICIs) compared to the fixed-in-space description. This holds true for the short-time dynamics up to $t = 1000$ fs. In contrast, for central frequencies higher than $\hbar\omega_c = 7.4$ eV the $|B, 0\rangle$ and $|X, 1\rangle$ states couple at many more frequencies, thereby diminishing the combined effects of rotation and LICIs, which results in dynamics nearly identical to the fixed-in-space model.

Finally, we explored the effect of varying the cavity decay rate and turning off the cavity leakage. In this scenario, only fixed-in-space molecules were considered. The results are presented in Fig. 7.

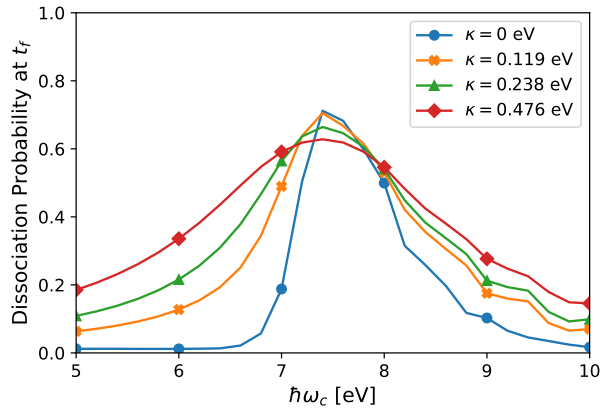


Figure 7: Dissociation probabilities (P_D) as a function of cavity central photon energy at $t_f = 1000$ fs obtained by the Lindblad master equation. Fixed-in-space molecules were applied for the case of several decay rates: $\kappa = 0$ eV ($\tau = \infty$), $\kappa = 0.119$ eV ($\tau \approx 5.52$ fs), $\kappa = 0.238$ eV ($\tau \approx 2.76$ fs) and $\kappa = 0.476$ eV ($\tau \approx 1.38$ fs). Other parameters are the same as in Fig. 5.

As the cavity decay rate κ decreases, the dissociation probability curve becomes narrower, although its maximum value increases slightly. The dissociation probability is at its narrowest when $\kappa = 0$, at which situation the dissociation probability reaches its maximum value. This is because, with a finite cavity lifetime which is inversely proportional to the decay rate, the photon energy broadens, causing photons with higher energies than the central frequency to appear. As a result, for a given central coupling frequency, dissociation can also

occur at energies below $\hbar\omega = 7.4 \text{ eV}$. The higher the cavity decay rate, the shorter the lifetime, and thus the broader the photon energy distribution. At $\kappa = 0$, however, dissociation almost completely disappears at frequencies lower than the central frequency $\hbar\omega_c = 7.4 \text{ eV}$, as the system cannot couple at those energies due to the absence of losses (infinite resonator lifetime). Consequently, the population cannot decay to the ground state $|X, 0\rangle$, but rather remains in the $|X, 1\rangle$ state, which is the photonic copy of the ground state, and dissociates from there. Due to the infinite cavity lifetime, the energy broadening vanishes entirely, and the resonance condition is perfectly satisfied, leading to the highest dissociation rate from the $|X, 1\rangle$ state.

For higher central frequencies, dissociation occurs at different magnitudes. In these cases, the $|X, 1\rangle$ and $|B, 0\rangle$ states always intersect, and the dynamics are determined by the coupling frequencies of the photon energy broadening in the lossy cavity. In the central frequency range $\hbar\omega_c = 7.4 \text{ eV} - 9 \text{ eV}$, the lossless and lossy cases differ significantly, with the lossless dissociation decaying earlier. In this range, the specific value of κ does not play a significant role. However, at higher frequencies, the dissociation rate increases with higher losses and shorter photon lifetimes.

It is noteworthy that dissociation still occurs even when $\kappa = 0$. This observation is consistent with the fact that the long-wavelength Floquet picture and the cavity description in the first excited state manifold are identical when the central frequency is the resonance frequency (i.e., when the two states are closest to each other). However, when higher excited states are included, the two descriptions are different.^{73,96}

Conclusions

We have explored the combined effects of molecular rotations and light-induced conical intersections (LICIs) on nonadiabatic quantum dynamics within a lossy cavity. Due to the bandwidth surrounding the central cavity frequency ω_c multiple light-induced conical

intersections can form, influencing the dynamics in ways that differ from the fixed-in-space description. The impact of LICIs depends on the relationship between the central cavity frequency and the resonance frequency between the $|X, 1\rangle$ and $|B, 0\rangle$ states. When the cavity central frequency is below $\hbar\omega_c = 7.4\text{ eV}$, the dissociation probability is reduced, while for frequencies above resonance, both the fixed-in-space and two-dimensional descriptions yield nearly identical results. Notably, due to energy broadening induced by cavity losses, dissociation also occurs at central frequencies well below the cavity resonance frequency.

Changes in the cavity lifetime—whether it decreases or increases—directly affect the loss rate. Larger loss rates result in greater photon energy broadening. This, in turn, alters the dissociation probability, either enhancing or diminishing it. In the extreme case where cavity losses vanish, the cavity lifetime becomes infinite. In this limit, with finite photon energy and within the framework of the first excited-state manifold, the behavior of the system is equivalent to the well-known Floquet description used in laser physics, which applies to continuous wave limits.

Acknowledgement

The authors are indebted to NKFIH for funding (Grant No. K146096). This paper was supported by the János Bolyai Research Scholarship of the Hungarian Academy of Sciences and the University of Debrecen Program for Scientific Publication. The authors thank Johannes Feist for valuable contributions. We appreciate fruitful discussions with Lorenz S. Cederbaum and Stéphane Guérin.

References

- (1) Hutchison, J. A.; Schwartz, T.; Genet, C.; Devaux, E.; Ebbesen, T. W. Modifying Chemical Landscapes by Coupling to Vacuum Fields. *Angew. Chem. Int. Ed.* **2012**, *51*, 1592–1596.

- (2) Chikkaraddy, R.; de Nijs, B.; Benz, F.; Barrow, S. J.; Scherman, O. A.; Rosta, E.; Demetriadou, A.; Fox, P.; Hess, O.; Baumberg, J. J. Single-molecule strong coupling at room temperature in plasmonic nanocavities. *Nature* **2016**, *535*, 127–130.
- (3) Ebbesen, T. W. Hybrid Light–Matter States in a Molecular and Material Science Perspective. *Acc. Chem. Res.* **2016**, *49*, 2403–2412.
- (4) Thomas, A.; George, J.; Shalabney, A.; Dryzhakov, M.; Varma, S. J.; Moran, J.; Chervy, T.; Zhong, X.; Devaux, E.; Genet, C. et al. Ground-State Chemical Reactivity under Vibrational Coupling to the Vacuum Electromagnetic Field. *Angew. Chem. Int. Ed.* **2016**, *55*, 11462–11466.
- (5) Vergauwe, R. M. A.; George, J.; Chervy, T.; Hutchison, J. A.; Shalabney, A.; Torbeev, V. Y.; Ebbesen, T. W. Quantum Strong Coupling with Protein Vibrational Modes. *J. Phys. Chem. Lett.* **2016**, *7*, 4159–4164.
- (6) Zhong, X.; Chervy, T.; Wang, S.; George, J.; Thomas, A.; Hutchison, J. A.; Devaux, E.; Genet, C.; Ebbesen, T. W. Non-Radiative Energy Transfer Mediated by Hybrid Light-Matter States. *Angew. Chem.* **2016**, *128*, 6310–6314.
- (7) Chervy, T.; Thomas, A.; Akiki, E.; Vergauwe, R. M. A.; Shalabney, A.; George, J.; Devaux, E.; Hutchison, J. A.; Genet, C.; Ebbesen, T. W. Vibro-Polaritonic IR Emission in the Strong Coupling Regime. *ACS Photonics* **2017**, *5*, 217–224.
- (8) Groenhof, G.; Toppari, J. J. Coherent Light Harvesting through Strong Coupling to Confined Light. *J. Phys. Chem. Lett.* **2018**, *9*, 4848–4851.
- (9) Damari, R.; Weinberg, O.; Krotkov, D.; Demina, N.; Akulov, K.; Golombek, A.; Schwartz, T.; Fleischer, S. Strong coupling of collective intermolecular vibrations in organic materials at terahertz frequencies. *Nat. Commun.* **2019**, *10*, 3248.

- (10) Ojambati, O.; Chikkaraddy, R.; Deacon, W.; Horton, M.; Kos, D.; Turek, V.; Keyser, U.; Baumberg, J. Quantum electrodynamics at room temperature coupling a single vibrating molecule with a plasmonic nanocavity. *Nat. Commun.* **2019**, *10*, 1049.
- (11) Rossi, T. P.; Shegai, T.; Erhart, P.; Antosiewicz, T. J. Strong plasmon-molecule coupling at the nanoscale revealed by first-principles modeling. *Nat. Commun.* **2019**, *10*, 3336.
- (12) Vergauwe, R. M. A.; Thomas, A.; Nagarajan, K.; Shalabney, A.; George, J.; Chervy, T.; Seidel, M.; Devaux, E.; Torbeev, V.; Ebbesen, T. W. Modification of Enzyme Activity by Vibrational Strong Coupling of Water. *Angew. Chem. Int. Ed.* **2019**, *58*, 15324–15328.
- (13) Jaber, A.; Reitz, M.; Singh, A.; Maleki, A.; Xin, Y.; Sullivan, B.; Dolgaleva, K. Hybrid architectures for terahertz molecular polaritonics. *Nat. Commun.* **2024**, *15*, 4427.
- (14) Galego, J.; Garcia-Vidal, F. J.; Feist, J. Cavity-induced modifications of molecular structure in the strong-coupling regime. *Phys. Rev. X* **2015**, *5*, 041022.
- (15) Galego, J.; Garcia-Vidal, F. J.; Feist, J. Suppressing photochemical reactions with quantized light fields. *Nat. Commun.* **2016**, *7*, 13841.
- (16) Kowalewski, M.; Bennett, K.; Mukamel, S. Cavity Femtochemistry: Manipulating Nonadiabatic Dynamics at Avoided Crossings. *J. Phys. Chem. Lett.* **2016**, *7*, 2050–2054.
- (17) Flick, J.; Appel, H.; Ruggenthaler, M.; Rubio, A. Cavity Born–Oppenheimer Approximation for Correlated Electron–Nuclear–Photon Systems. *J. Chem. Theory Comput.* **2017**, *13*, 1616–1625.

- (18) Herrera, F.; Spano, F. Dark Vibronic Polaritons and the Spectroscopy of Organic Microcavities. *Phys. Rev. Lett.* **2017**, *118*, 223601.
- (19) Feist, J.; Galego, J.; Garcia-Vidal, F. J. Polaritonic Chemistry with Organic Molecules. *ACS Photonics* **2018**, *5*, 205–216.
- (20) del Pino, J.; Schröder, F. A. Y. N.; Chin, A. W.; Feist, J.; Garcia-Vidal, F. J. Tensor Network Simulation of Non-Markovian Dynamics in Organic Polaritons. *Phys. Rev. Lett.* **2018**, *121*, 227401.
- (21) Ruggenthaler, M.; Tancogne-Dejean, N.; Flick, J.; Appel, H.; Rubio, A. From a quantum-electrodynamical light–matter description to novel spectroscopies. *Nat. Rev. Chem.* **2018**, *2*, 0118.
- (22) Szidarovszky, T.; Halász, G. J.; Császár, A. G.; Cederbaum, L. S.; Vibók, Á. Conical Intersections Induced by Quantum Light: Field-Dressed Spectra from the Weak to the Ultrastrong Coupling Regimes. *J. Phys. Chem. Lett.* **2018**, *9*, 6215–6223.
- (23) Vendrell, O. Collective Jahn-Teller Interactions through Light-Matter Coupling in a Cavity. *Phys. Rev. Lett.* **2018**, *121*, 253001.
- (24) Reitz, M.; Sommer, C.; Genes, C. Langevin Approach to Quantum Optics with Molecules. *Phys. Rev. Lett.* **2019**, *122*, 203602.
- (25) Triana, J. F.; Sanz-Vicario, J. L. Revealing the Presence of Potential Crossings in Diatomics Induced by Quantum Cavity Radiation. *Phys. Rev. Lett.* **2019**, *122*, 063603.
- (26) Huang, C.; Ahrens, A.; Beutel, M.; Varga, K. Two electrons in harmonic confinement coupled to light in a cavity. *Phys. Rev. B* **2021**, *104*, 165147.
- (27) Triana, J.; Sanz-Vicario, J. Polar diatomic molecules in optical cavities: Photon scaling, rotational effects, and comparison with classical fields. *J. Chem. Phys.* **2021**, *154*, 094120.

- (28) Riso, R. R.; Haugland, T. S.; Ronca, E.; Koch, H. On the characteristic features of ionization in QED environments. *J. Chem. Phys.* **2022**, *156*, 234103.
- (29) Malave, J.; Aklilu, Y. S.; Beutel, M.; Huang, C.; Varga, K. Harmonically confined N -electron systems coupled to light in a cavity. *Phys. Rev. B* **2022**, *105*, 115127.
- (30) Fábri, C. Practical guide to the statistical mechanics of molecular polaritons. *Mol. Phys.* **2024**, *122*, e2272691.
- (31) Schnappinger, T.; Kowalewski, M. Ab Initio Vibro-Polaritonic Spectra in Strongly Coupled Cavity-Molecule Systems. *J. Chem. Theory Comput.* **2023**, *19*, 9278–9289.
- (32) Schnappinger, T.; Kowalewski, M. Nonadiabatic Wave Packet Dynamics with Ab Initio Cavity-Born-Oppenheimer Potential Energy Surfaces. *J. Chem. Theory Comput.* **2023**, *19*, 460–471.
- (33) Schnappinger, T.; Sidler, D.; Ruggenthaler, M.; Rubio, A.; Kowalewski, M. Cavity Born–Oppenheimer Hartree–Fock Ansatz: Light–Matter Properties of Strongly Coupled Molecular Ensembles. *J. Phys. Chem. Lett.* **2023**, *14*, 8024–8033.
- (34) Szidarovszky, T. Pauli Principle in Polaritonic Chemistry. *Phys. Rev. A* **2023**, *108*, 053118.
- (35) Szidarovszky, T. An Efficient and Flexible Approach for Computing Rovibrational Polaritons from First Principles. *J. Chem. Phys.* **2023**, *159*, 014112.
- (36) Fiechter, M. R.; Richardson, J. O. Understanding the cavity Born–Oppenheimer approximation. *J. Chem. Phys.* **2024**, *160*, 184107.
- (37) Sokolovskii, I.; Groenhof, G. Non–Hermitian molecular dynamics simulations of exciton-polaritons in lossy cavities. *J. Chem. Phys.* **2024**, *160*, 092501.

- (38) Bassler, N. S.; Reitz, M.; Holzinger, R.; Vibók, Á.; Halász, G. J.; Gurlek, B.; Genes, C. Generalized energy gap law: An open system dynamics approach to non-adiabatic phenomena in molecules. Submitted to arXiv [quant-ph] on 2024-05-14, <https://arxiv.org/abs/2405.08718>, accessed 2025-02-28.
- (39) Szidarovszky, T. Ab initio study on the dynamics and spectroscopy of collective rovibrational polaritons. *J. Chem. Phys.* **2025**, *162*, 034117.
- (40) Fábri, C.; Halász, G. J.; Hofierka, J.; Cederbaum, L. S.; Vibók, Á. Impact of Dipole Self-Energy on Cavity-Induced Nonadiabatic Dynamics. *J. Chem. Theory Comput.* **2025**, *21*, 575–589.
- (41) Sandik, G.; Feist, J.; García-Vidal, F. J.; Schwartz, T. Cavity-enhanced energy transport in molecular systems. *Nat. Mater.* **2025**, *24*, 344–355.
- (42) Wang, D. Cavity quantum electrodynamics with a single molecule: Purcell enhancement, strong coupling and single-photon nonlinearity. *J. Phys. B: At. Mol. Opt. Phys.* **2021**, *54*, 133001.
- (43) Du, M.; Martínez-Martínez, L. A.; Ribeiro, R. F.; Hu, Z.; Menon, V. M.; Yuen-Zhou, J. Theory for polariton-assisted remote energy transfer. *Chem. Sci.* **2018**, *9*, 6659–6669.
- (44) Li, T. E.; Nitzan, A.; Subotnik, J. E. Collective Vibrational Strong Coupling Effects on Molecular Vibrational Relaxation and Energy Transfer: Numerical Insights via Cavity Molecular Dynamics Simulations. *Angew. Chem. Int. Ed.* **2021**, *60*, 15533–15540.
- (45) Semenov, A.; Nitzan, A. Electron transfer in confined electromagnetic fields. *J. Chem. Phys.* **2019**, *150*, 174122.
- (46) Mandal, A.; Krauss, T. D.; Huo, P. Polariton-Mediated Electron Transfer via Cavity Quantum Electrodynamics. *J. Phys. Chem. B* **2020**, *124*, 6321–6340.

- (47) Wellnitz, D.; Pupillo, G.; Schachenmayer, J. A quantum optics approach to photoinduced electron transfer in cavities. *J. Chem. Phys.* **2021**, *154*, 054104.
- (48) Campos-Gonzalez-Angulo, J. A.; Ribeiro, R. F.; Yuen-Zhou, J. Resonant catalysis of thermally activated chemical reactions with vibrational polaritons. *Nat. Commun.* **2019**, *10*, 4685.
- (49) Galego, J.; Climent, C.; Garcia-Vidal, F. J.; Feist, J. Cavity Casimir-Polder Forces and Their Effects in Ground-State Chemical Reactivity. *Phys. Rev. X* **2019**, *9*, 021057.
- (50) Li, T. E.; Cui, B.; Subotnik, J. E.; Nitzan, A. Molecular Polaritonics: Chemical Dynamics Under Strong Light-Matter Coupling. *Annu. Rev. Phys. Chem.* **2022**, *73*, 43–71.
- (51) Fregoni, J.; Corni, S. In *Theoretical and Computational Photochemistry*; García-Iriepa, C., Marazzi, M., Eds.; Elsevier, 2023; Chapter 7 - Polaritonic Chemistry, pp 191–211.
- (52) Felicetti, S.; Fregoni, J.; Schnappinger, T.; Reiter, S.; De Vivie-Riedle, R.; Feist, J. Photoprotecting Uracil by Coupling with Lossy Nanocavities. *J. Phys. Chem. Lett.* **2020**, *11*, 8810–8818.
- (53) Fregoni, J.; Corni, S.; Persico, M.; Granucci, G. Photochemistry in the strong coupling regime: A trajectory surface hopping scheme. *J. Comput. Chem.* **2020**, *41*, 2033–2044.
- (54) Fregoni, J.; Granucci, G.; Coccia, E.; Persico, M.; Corni, S. Manipulating azobenzene photoisomerization through strong light–molecule coupling. *Nat. Commun.* **2018**, *9*, 4688.
- (55) Fregoni, J.; Granucci, G.; Persico, M.; Corni, S. Strong Coupling with Light Enhances the Photoisomerization Quantum Yield of Azobenzene. *Chem* **2020**, *6*, 250–265.
- (56) Davidsson, E.; Kowalewski, M. Simulating photodissociation reactions in bad cavities with the Lindblad equation. *J. Chem. Phys.* **2020**, *153*, 234304.

- (57) Torres-Sánchez, J.; Feist, J. Molecular photodissociation enabled by ultrafast plasmon decay. *J. Chem. Phys.* **2021**, *154*, 014303.
- (58) Fábri, C.; Halász, G. J.; Cederbaum, L. S.; Vibók, Á. Impact of Cavity on Molecular Ionization Spectra. *J. Phys. Chem. Lett.* **2024**, *15*, 4655–4661.
- (59) Cederbaum, L. S.; Fedyk, J. Making molecules in cavity. *J. Chem. Phys.* **2024**, *161*, 074303.
- (60) Csehi, A.; Halász, G. J.; Cederbaum, L. S.; Vibók, Á. Competition between Light-Induced and Intrinsic Nonadiabatic Phenomena in Diatomics. *J. Phys. Chem. Lett.* **2017**, *8*, 1624–1630.
- (61) Csehi, A.; Kowalewski, M.; Halász, G. J.; Vibók, Á. Ultrafast dynamics in the vicinity of quantum light-induced conical intersections. *New J. Phys.* **2019**, *21*, 093040.
- (62) Gu, B.; Mukamel, S. Manipulating nonadiabatic conical intersection dynamics by optical cavities. *Chem. Sci.* **2020**, *11*, 1290–1298.
- (63) Gu, B.; Mukamel, S. Cooperative Conical Intersection Dynamics of Two Pyrazine Molecules in an Optical Cavity. *J. Phys. Chem. Lett.* **2020**, *11*, 5555–5562.
- (64) Szidarovszky, T.; Halász, G. J.; Vibók, Á. Three-player polaritons: nonadiabatic fingerprints in an entangled atom-molecule-photon system. *New J. Phys.* **2020**, *22*, 053001.
- (65) Farag, M. H.; Mandal, A.; Huo, P. Polariton induced conical intersection and Berry phase. *Phys. Chem. Chem. Phys.* **2021**, *23*, 16868–16879.
- (66) Szidarovszky, T.; Badankó, P.; Halász, G.; Vibók, Á. Nonadiabatic phenomena in molecular vibrational polaritons. *J. Chem. Phys.* **2021**, *154*, 064305.
- (67) Badankó, P.; Umarov, O.; Fábri, C.; Halász, G. J.; Vibók, Á. Topological aspects of cavity-induced degeneracies in polyatomic molecules. *Int. J. Quantum Chem.* **2022**, *122*, e26750.

- (68) Csehi, A.; Vendrell, O.; Halász, G. J.; Vibók, Á. Competition between collective and individual conical intersection dynamics in an optical cavity. *New J. Phys.* **2022**, *24*, 073022.
- (69) Fábri, C.; Halász, G. J.; Cederbaum, L. S.; Vibók, Á. Radiative emission of polaritons controlled by light-induced geometric phase. *Chem. Commun.* **2022**, *58*, 12612–12615.
- (70) Fábri, C.; Halász, G. J.; Vibók, Á. Probing Light-Induced Conical Intersections by Monitoring Multidimensional Polaritonic Surfaces. *J. Phys. Chem. Lett.* **2022**, *13*, 1172–1179.
- (71) Fischer, E. W.; Saalfrank, P. Cavity-induced non-adiabatic dynamics and spectroscopy of molecular rovibrational polaritons studied by multi-mode quantum models. *J. Chem. Phys.* **2022**, *157*, 034305.
- (72) Han, S.; Xie, C.; Hu, X.; Yarkony, D. R.; Guo, H.; Xie, D. Quantum Dynamics of Photodissociation: Recent Advances and Challenges. *J. Phys. Chem. Lett.* **2023**, *14*, 10517–10530.
- (73) Fábri, C.; Csehi, A.; Halász, G. J.; Cederbaum, L. S.; Vibók, Á. Classical and quantum light-induced non-adiabaticity in molecular systems. *AVS Quantum Sci.* **2024**, *6*, 023501.
- (74) Warren, S.; Wang, Y.; Benavides-Riveros, C. L.; Mazziotti, D. A. Quantum algorithm for polaritonic chemistry based on an exact ansatz. *Quantum Sci. Technol.* **2025**, *10*, 02LT02.
- (75) Moiseyev, N.; Šindelka, M.; Cederbaum, L. S. Laser-induced conical intersections in molecular optical lattices. *J. Phys. B: At. Mol. Opt. Phys.* **2008**, *41*, 221001.
- (76) Šindelka, M.; Moiseyev, N.; Cederbaum, L. S. Strong impact of light-induced conical

- intersections on the spectrum of diatomic molecules. *J. Phys. B: At. Mol. Opt. Phys.* **2011**, *44*, 045603.
- (77) Halász, G. J.; Vibók, Á.; Cederbaum, L. S. Direct Signature of Light-Induced Conical Intersections in Diatomics. *J. Phys. Chem. Lett.* **2015**, *6*, 348–354.
- (78) Natan, A.; Ware, M. R.; Prabhudesai, V. S.; Lev, U.; Bruner, B. D.; Heber, O.; Bucksbaum, P. H. Observation of Quantum Interferences via Light-Induced Conical Intersections in Diatomic Molecules. *Phys. Rev. Lett.* **2016**, *116*, 143004.
- (79) Fábri, C.; Halász, G. J.; Cederbaum, L. S.; Vibók, Á. Born-Oppenheimer approximation in optical cavities: From success to breakdown. *Chem. Sci.* **2021**, *12*, 1251–1258.
- (80) Fábri, C.; Halász, G. J.; Cederbaum, L. S.; Vibók, Á. Signatures of light-induced nonadiabaticity in the field-dressed vibronic spectrum of formaldehyde. *J. Chem. Phys.* **2021**, *154*, 124308.
- (81) Ulusoy, I. S.; Vendrell, O. Dynamics and spectroscopy of molecular ensembles in a lossy microcavity. *J. Chem. Phys.* **2020**, *153*, 044108.
- (82) Silva, R.; Pino, J.; García-Vidal, F.; Feist, J. Polaritonic molecular clock for all-optical ultrafast imaging of wavepacket dynamics without probe pulses. *Nat. Commun.* **2020**, *11*, 1423.
- (83) Manzano, D. A short introduction to the Lindblad master equation. *AIP Adv.* **2020**, *10*, 025106.
- (84) Fábri, C.; Császár, A. G.; Halász, G. J.; Cederbaum, L. S.; Vibók, Á. Coupling polyatomic molecules to lossy nanocavities: Lindblad vs Schrödinger description. *J. Chem. Phys.* **2024**, *160*, 214308.
- (85) Wolniewicz, L.; Staszewska, G. ${}^1\Sigma_u^+ \rightarrow X^1\Sigma_g^+$ transition moments for the hydrogen molecule. *J. Mol. Spectrosc.* **2003**, *217*, 181–185.

- (86) Pachucki, K. Born-Oppenheimer potential for H₂. *Phys. Rev. A* **2010**, *82*, 032509.
- (87) Siłkowski, M.; Zientkiewicz, M.; Pachucki, K. *New Electron Correlation Methods and their Applications, and Use of Atomic Orbitals with Exponential Asymptotes*; Elsevier, 2021; Chapter Twelve - Accurate Born-Oppenheimer potentials for excited Σ^+ states of the hydrogen molecule, pp 255–267.
- (88) Johansson, J.; Nation, P.; Nori, F. QuTiP: An open-source Python framework for the dynamics of open quantum systems. *Comput. Phys. Commun.* **2012**, *183*, 1760–1772.
- (89) Johansson, J.; Nation, P.; Nori, F. QuTiP 2: A Python framework for the dynamics of open quantum systems. *Comput. Phys. Commun.* **2013**, *184*, 1234–1240.
- (90) Light, J. C.; Carrington Jr., T. Discrete-Variable Representations and their Utilization. *Adv. Chem. Phys.* **2000**, *114*, 263–310.
- (91) Visser, P. M.; Nienhuis, G. Solution of quantum master equations in terms of a non-Hermitian Hamiltonian. *Phys. Rev. A* **1995**, *52*, 4727–4736.
- (92) Meyer, H.-D.; Manthe, U.; Cederbaum, L. The multi-configurational time-dependent Hartree approach. *Chem. Phys. Lett.* **1990**, *165*, 73–78.
- (93) Beck, M.; Jäckle, A.; Worth, G.; Meyer, H.-D. The multiconfiguration time-dependent Hartree (MCTDH) method: a highly efficient algorithm for propagating wavepackets. *Phys. Rep.* **2000**, *324*, 1–105.
- (94) Sakurai, J. J. *Modern quantum mechanics; rev. ed.*; Addison-Wesley: Reading, MA, 1994.
- (95) Saharyan, A.; Rousseaux, B.; Kis, Z.; Stryzhenko, S.; Guérin, S. Propagating single photons from an open cavity: Description from universal quantization. *Phys. Rev. Res.* **2023**, *5*, 033056.

- (96) Avanesian, C.; Wang, Y.; Yarkony, D. R. Floquet-Engineered Photodissociation Simulated Using Coupled Potential Energy and Dipole Matrices. *J. Phys. Chem. Lett.* **2024**, *15*, 9905–9911.

TOC Graphic

